

# Reconstruction of 3D Accident Sites Using USGS LiDAR, Aerial Images, and Photogrammetry

Toby Terpstra, Jordan Dickinson, Alireza Hashemian, and Stephen Fenton Kineticorp LLC

Citation: Terpstra, T., Dickinson, J., Hashemian, A., and Fenton, S., "Reconstruction of 3D Accident Sites Using USGS LiDAR, Aerial Images, and Photogrammetry," SAE Technical Paper 2019-01-0423, 2019, doi:10.4271/2019-01-0423.

#### **Abstract**

he accident reconstruction community has previously relied upon photographs and site visits to recreate a scene. This method is difficult in instances where the site has changed or is not accessible. In 2017 the United States Geological Survey (USGS) released historical 3D point clouds (LiDAR) allowing for access to digital 3D data without visiting the site. This offers many unique benefits to the reconstruction community including: safety, budget, time, and historical preservation. This paper presents a methodology for collecting this data and using it in conjunction with aerial imagery, and camera matching photogrammetry to create 3D computer models of the scene without a site visit. To determine accuracies achievable using this method, evidence locations solved

for using only USGS LiDAR, aerial images and scene photographs (representative of emergency personnel photographs) were compared with known locations documented using total station survey equipment and ground-based 3D laser scanning. The data collected from three different site locations was analyzed, and camera matching photogrammetry was performed independently by 5 different individuals to locate evidence. On average, the resulting evidence for all three test sites was found to be within 3.0 inches (8cm) of known evidence locations with a standard deviation of 1.7 inches (4cm). To further evaluate the quality of the USGS LiDAR, a comparative point cloud analysis of the roadway surfaces was performed. On average, 85% of the USGS LiDAR points were found to be within .5 inches of the ground-based 3D scanning points.

### Introduction / Background

Traditionally, creating a 3D computer model of an incident site has required a visit to the incident site to inspect, measure, and document both the site geometry as well as any existing evidence [1, 2, 3, 4, 5, 6, 7, 8, 9]. Although there are many benefits to a physical site inspection, there are instances when a typical site inspection may be impractical or unsafe. Some of the difficulties that an investigator may experience related to site visits include:

- Limited or no access to site
- Significant site changes
- · Budget / time at site

When significant site updates have been made since the time of the incident and opportunity for inspection, such as construction or the relocation of a roadway, site inspections may prove to be of little benefit. In these instances, historical data representative of the time of incident becomes invaluable. When vehicular accidents occur on an overpass or bridge, access to safely inspecting the incident site can become limited or impractical. Scheduling, budget concerns and timing can also play a role in the accessibility of a site

for inspection. Using aerial imagery, USGS LiDAR, and camera matching photogrammetry in combination the methodology presented demonstrates opportunity to create a 3D site model representative of the time of incident, without a physical site inspection.

## **Aerial Imagery**

Historical aerial photographs, available from several online sources, have been and continue to be invaluable to the accident reconstruction community. While some regions have limited aerial imagery available, regions where multiple dates at high resolution is available offer a specific advantage to creating accurate 3D models of incident sites. This imagery can be used for determining changes to the incident site, incorporating historical site features such as roadway striping from time of incident, and locating evidence such as furrows, tire marks, gouge marks, fluid spill areas, and burn areas visible within the imagery. Aerial imagery can also be used as a background image or mapped texture to create a photorealistic representation of the incident site on which evidence

can be placed to create a forensic scene recreation easily understood by any audience [10].

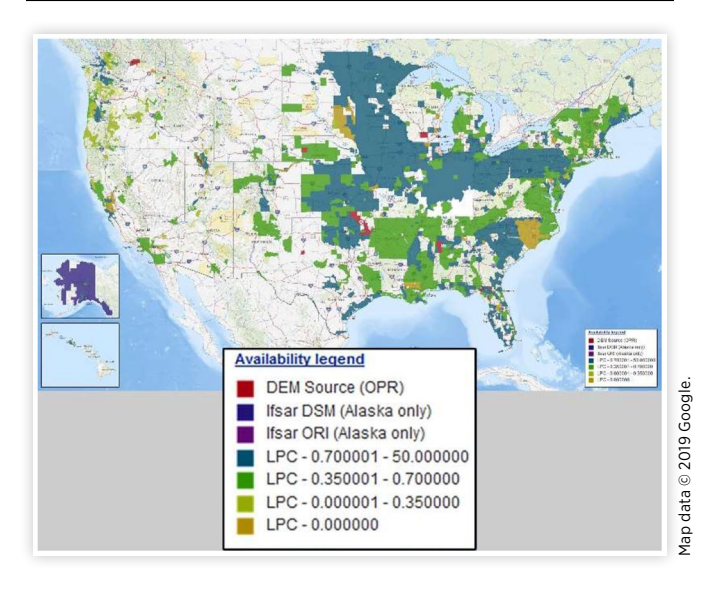
#### **USGS LIDAR**

The word LiDAR is a combination of two words, light and radar, but it is commonly accepted as an acronym for Light Detection and Ranging [11,12]. In 2015, the United States Geological Survey (USGS) began providing LiDAR based, 3D point clouds publicly [13]. The USGS begin the 3D Elevation Program (3DEP) in 2012 as an eight-year program for mapping the United States and the U.S. territories. Similar to aerial imagery, this resource does not have the same coverage in all areas. However, the USGS data collection process is ongoing and there are already regions where this LiDAR data has been collected on multiple dates allowing for a three-dimensional comparison of changes to an incident site. To assess availability of data and resolution, there is a map on the USGS 3DEP website that includes a legend for lidar point clouds (LPC) coverage areas with a unique color for each resolution range in points per meter (Figure 1).

USGS LiDAR data is an excellent resource for the accident reconstruction community. It shows potential to be used in many ways including:

- Evaluating changes to incident sites in 3D
- Determining roadway grade and cross-slope
- Determining crest of a hill and line of sight
- Creating surfaced 3D terrains for simulation purposes
- Extending 3D models of incident sites to include surrounding areas
- Improving photogrammetric solution accuracy
- Supplementing incomplete site inspection data
- Creating 3D models for sites with limited access

**FIGURE 1** USGS LiDAR coverage through 3DEP as of December 2018.



Previous research has shown that photogrammetric solutions can be improved upon by utilizing USGS LiDAR to for landmarks and terrain features that would be impractical to document during a site inspection with typical surveying and scanning equipment  $[\underline{14}]$ .

Another potential benefit is a time and cost savings. In instances where there is little benefit from a site inspection beyond determining and documenting the slope or percent grade of the roadway, USGS LiDAR might prove to be a suitable substitute for a time consuming and expensive trip.

## Camera Matching Photogrammetry

Camera matching photogrammetry is a close-range photogrammetry method. It utilizes the principles of reverse camera projection within 3D software to locate three-dimensional positions of evidence from photographs or video. In general, the camera matching process involves the following:

- 1. Review of photographs and or video for both evidence to be located and other scene features that will be useful for alignment.
- 2. Obtain 2D aerial images for recreating site features. These can typically be retrieved from online resources that indicate the date the images were recorded. (This step may not be needed if a site visit will be performed and no site features have changed since the time of incident, such as a repaving and restriping of the roadway.)
- 3. Obtain 3D data of the site by recording during a site visit, having provided by another party who has visited the site, or downloading from online resources.
- 4. Process and format the 3D data to be compatible with 3D modeling software to be used in camera matching. This includes translation of useful 2D information onto 3D surfaces.
- 5. Create a 3D environment by importing the 3D site data into the 3D modeling software.
- 6. Analyze and correct for lens distortion from photographs or video frames as needed.
- 7. Set the photograph or video frame as a viewport background in the 3D modeling software.
- 8. Create a virtual camera in the 3D environment and adjust the camera position, orientation, and field of view until an alignment between the 3D environment and the background image is achieved, utilizing the full resolution of the imagery, and ideally repeating this step with multiple photographs.
- 9. Place evidence within the environment such that it is aligned with the photograph or video frame and either consistent with multiple cameras or with a single camera on a known surface.
- 10. Peer review of saved camera match images and evidence placement.
- 11. Save imagery to validate matches and evidence placement.

The process can be repeated for multiple images to determine motion over time, to place additional evidence in other areas of the scene, or to further verify the location of placed evidence from additional vantages. This photogrammetry method is well accepted in the incident reconstruction community. It has been used for many purposes including: 3D site reconstruction [1, 2, 3, 4, 5, 6, 7, 8, 9], vehicle modeling and crush depth [15, 16, 17, 18, 19, 20, 21, 22, 23, 24, 25, 26], determining velocity and path of travel [9, 27, 28, 29], projection mapping [30, 31], and photo scanning [32, 33, 34, 35, 36].

In combination, USGS LiDAR data, aerial imagery, and photographs or video from time of incident can be used to create an accurate 3D scene reconstruction or model. The methodology presented in this paper describes how to incorporate roadway markings and other scene features from aerial images, evidence visible in historical aerial imagery, evidence visible in photographs and video from time of incident, and 3D USGS LiDAR data in both surfaced and point cloud formats to create a 3D model of an incident site that represents the time of incident. The accuracy with which this can be accomplished is described within the results and conclusions section.

**FIGURE 2** Site locations 1, 2, and 3 in order from top to bottom.



## **Methodology**

## **Testing Sites**

For the purposes of this study, three different sites were selected for analysis. These sites were chosen for their proximity and accessibility, and because it was known that USGS LiDAR was available. They all offer unique features as well. The first site can be classified as an urban residential area. The second site is an urban business area, and the third site was chosen within a state park and is more rural in nature (Figure 2).

#### **Evidence Placement**

To simulate evidence documented by police or emergency personnel at an incident site, five markings were placed on the roadway surface at each site using green spray chalk. A 2018 Nissan Leaf was also parked at each site to represent a vehicle point of rest. These were then photographed from various locations using a Canon EOS 5D Mark II with a 24-105mm lens. All photographs to be used for camera matching photogrammetry were taken with a lens setting of 24mm.

#### **Baseline Data Collection**

A Sokkia Set5 30R total station was used with a prism to document the spray chalk locations and a FARO Focus S 350 3D laser scanner was used to document the location and orientation of the vehicle. This established known locations and positions which were then used as the baseline for comparing the accuracy of other solutions (Figure 3).

**FIGURE 3** Recording locations of spray chalk and vehicle using a total station and 3D laser scanning.



# Creating USGS LiDAR Based 3D Environments

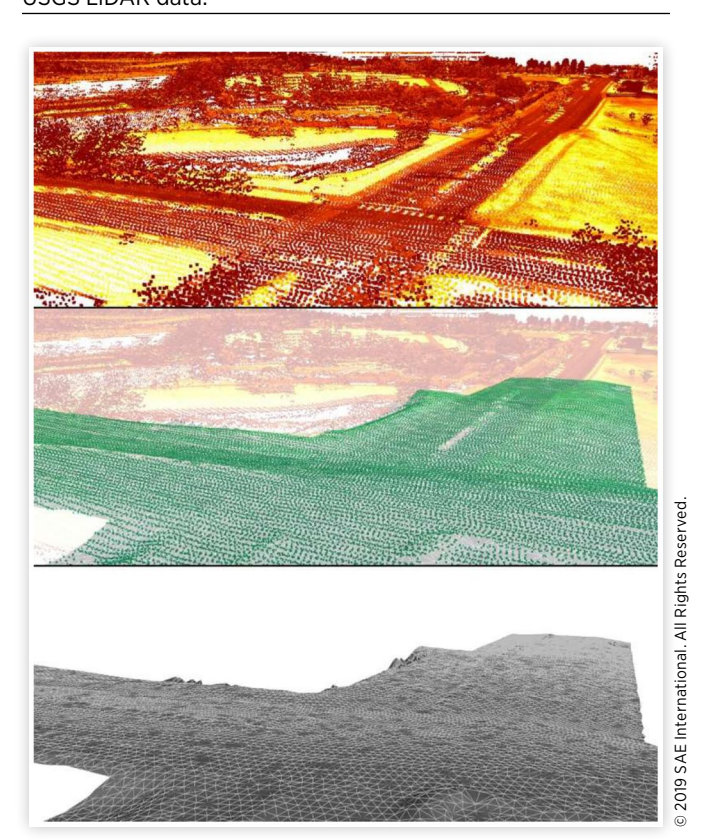
USGS LiDAR data was selected and downloaded for each of the three site locations. At each location, multiple collection dates (2008 and 2013) were available. Both data sets were available within the same resolution range (0.350001m - 0.700000m) as specified by USGS and the more recent date was used to minimize differences in the scenes from time of USGS LiDAR acquisition and site visit. After downloading

the USGS LiDAR data in ".LAS" file format, the point clouds were imported into CloudCompare v. 2.9.1 [37] where the point clouds were colorized based on intensity values stored within the scalar properties. The intensity values are stored as a grey scale value from white to black depending on the amount of return energy measured during capture and can be colorized based on any gradient chosen within the software. Viewing the point cloud with intensity values makes it easier to distinguish lane lines as well based on their retro-reflective material and higher energy return relative to surrounding surfaces [38]. The intensity colorized USGS LiDAR point cloud data was then converted into ".rcs" format using Autodesk ReCap v.1.0 for use in Autodesk 3ds Max 2017, and Autodesk AutoCAD 2017. It is worth noting that other file formats may be required if working within alternate 3D modeling software.

A terrain mesh was then created using an isolated portion of the same USGS LiDAR data. Using CloudCompare v.2.9.1, areas farther from the center of the site were cropped out or removed, as were points off of the roadway area. Outlier points that can be described as individual points or "islands" were visually detected and removed from the point cloud. The statistical outlier removal (SOR) function may also be useful for additional filtering, but it was not used in this study. The point cloud was then subsampled using a 1m value to create a less dense point cloud. The resulting point cloud was then surfaced in CloudCompare, creating a 3D mesh (Figure 4).

Aerial imagery was then downloaded using CAD-Earth v5.1.14. This software uses Google Earth imagery and is

**FIGURE 4** 1) USGS LiDAR point cloud with red to yellow gradient for intensity values, 2) Terrain point cloud subsampled to 1m, 3) Resulting mesh terrain built from the subsampled USGS LiDAR data.

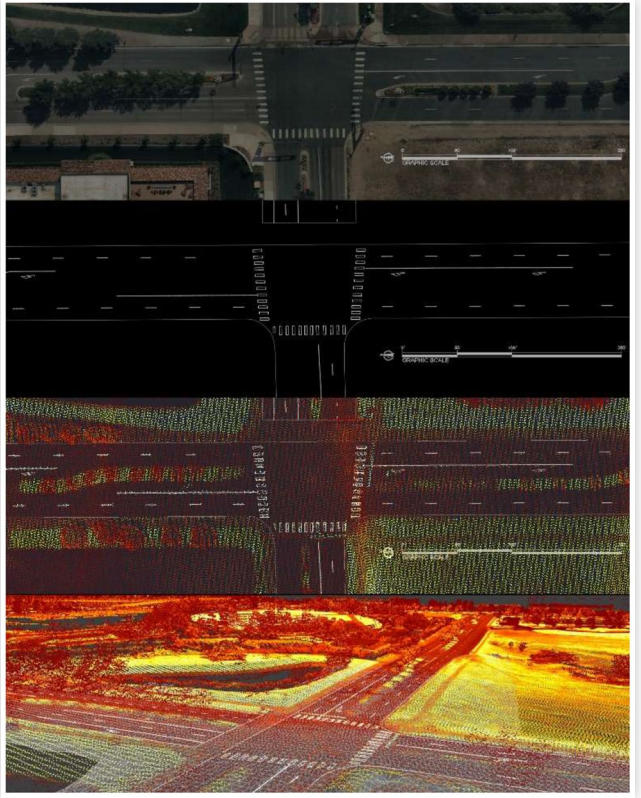


especially useful in processes that don't involve a site visit as the aerial imagery is automatically imported into AutoCAD at the correct scale. To take advantage of higher resolution aerial imagery available through other sources, NearMap, a browser-based software, was used. This higher resolution aerial was scaled and aligned to the Google aerial image from CAD-Earth with a known scale. The aerial images were then aligned to USGS LiDAR data using the intensity colorization as a reference. Once aligned, roadway markings were traced on top of the aerial imagery creating 2D vector-based lines. To complete the 3D environment, the 2D aerial traced lines were projected down to the 3D mesh created from USGS LiDAR within Autodesk 3ds Max. This projection can be accomplished using various tools including shape merging and the free Glue Utility from iToo Software [39] (Figure 4).5

## **Evidence Locations from Photogrammetry**

Camera matching photogrammetry was used to solve for the locations of the spray chalk marks as well as the vehicle location and orientation. Five individuals performed the camera matching process and solved for evidence locations at all three sites. To do this they were given Autodesk 3ds Max files for each site. These files included the USGS LiDAR point cloud colorized with intensity values, the mesh terrain based

FIGURE 5 From top to bottom, 1) NearMap aerial image, 2) 2D vector lines traced on aerial image, 3) Aerial traced 2D vector lines and USGS LiDAR, 4) Resulting 3D environment with vector lines projected onto surfaced ground mesh.



2019 SAE International. All Rights Reserved

on 1m spacing from the USGS LiDAR, 3D line work or splines from traced aerial imagery, that were glued to the terrain mesh, and a site photograph set as a viewport background. The file also contained a mesh and point cloud of the vehicle as well as a virtual camera. The subject vehicle, a 2018 Nissan Leaf, was scanned using a FARO Focus S 350 3D laser scanner from multiple locations resulting in a point cloud with over 14 million 3D points and good overall vehicle coverage. A vehicle mesh model was purchased online and the overall scale and vehicle proportions were adjusted to match the 3D scan data. The camera and vehicle were arbitrarily placed outside of the site environment. As part of the camera matching process, individuals then adjusted the camera position, orientation, and field of view until an alignment between the 3D environment and the background image was achieved. They then placed splines on the mesh terrain surface to indicate the spray chalk locations and translated and rotated the vehicle mesh until it was aligned to the photograph. Initially the participants were only given one photograph to solve for at each site. Their resulting evidence placements were recorded for comparison to the known evidence locations and orientations. They were then given two additional photographs for each site. After camera matching the additional two photographs, each individual reevaluated evidence placements for all five spray chalk marks and the vehicle location and orientation until they believed they had achieved evidence placements what were consistent with all three camera matches. These three-photograph solutions were then recorded for comparison to the known evidence locations and orientations (Figure 6).

photograph, Bottom: Camera matching photogrammetry photograph, Bottom: Camera matched solution with USGS LiDAR based 3D environment viewed through the virtual camera. Evidence placements are also visible with blue linework for the roadway spray chalk, and both geometric mesh and point cloud visible for the vehicle placement (Additional examples of the camera match solutions available in Appendix A).



### **Overview of Methodology**

The processes described in this methodology can be summarized in the following steps:

- 1. Download, (<a href="https://viewer.nationalmap.gov/basic/">https://viewer.nationalmap.gov/basic/</a>) colorize, and convert USGS LiDAR point cloud.
- 2. Create surfaced mesh of the terrain using a subsampled portion USGS LiDAR data.
- 3. Download aerial imagery, preferably using CAD-Earth software to establish a known scale.
- 4. Trace roadway markings and features from aerial, creating 2D vector-based lines.
- 5. Project the 2D vector-based lines onto the 3D surfaced terrain
- Create 3D environment to include USGS LiDAR point cloud, surfaced mesh of terrain, and 3D lines of roadway markings.
- 7. Analyze photographs to be used and correct for lens distortion if needed.
- 8. Use camera matching photogrammetry to achieve an alignment of the 3D environment to the photograph, use multiple photographs where possible.
- Based on the photogrammetry solution, place shapes or geometry to represent evidence within the 3D environment, such that it is consistent with all camera matches.
- 10. Peer review of results.

#### **Results**

#### Site-01: LiDAR Comparison

To evaluate the accuracy of the USGS LiDAR in comparison to traditionally collected LiDAR or ground-based LiDAR, a distance comparison was performed. For this comparison, a section of overlapping data from both the USGS LiDAR and the ground-based LiDAR was chosen. This section was approximately 96ft (29m) long and 34ft (10m) wide (Figure 7).

Within the selected area the ground-based LiDAR data contained 975,153 points for a resolution of approximately 301 points ft² (3,244 points m²). The USGS LiDAR data contained 1,136 points for a resolution of approximately 0.4 ft² (3.9 points m²). The distance comparison was performed in CloudCompare [39] using the compute cloud distance tool. This tool evaluates the distance between points of one 3D point cloud to another based on the a nearest neighbor. All distance measurements include both horizontal and vertical distances between the two point clouds. When the USGS point cloud and the ground-based point clouds were compared, approximately 44% of the points were found to be within 0.6in, approximately 84% of the points were found to be within 1.2in, and approximately 98% of the points were found to be within 1.8in (Table 1).

FIGURE 7 Orthographic top view of site 1 showing the area used for terrain comparison. The grayscale area represents the ground-based LiDAR point cloud, the red and orange colored points represent the USGS LiDAR outside of the comparison area. The USGS LiDAR points that were used in comparison are colorized based on distance away from the ground-based LiDAR data set (Distances by color shown in Table 1).

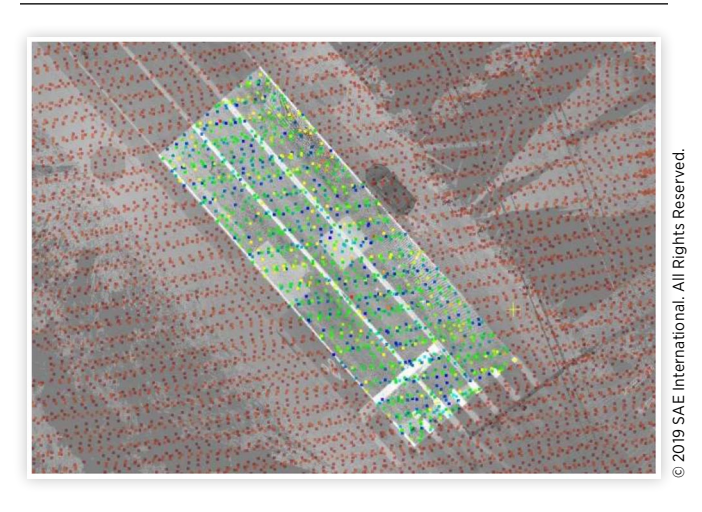
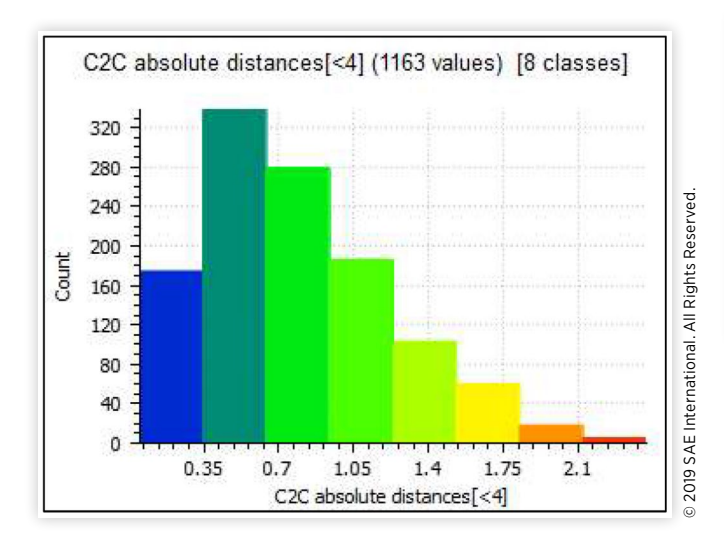


TABLE 1 A histogram showing USGS LiDAR point cloud distances (inches) from ground-based LiDAR points.



### Site-01: Photogrammetry

At the first site, the average distance for placing the spray chalk marks and for the center location of the vehicle from known locations for all five participants was 5.8in (15cm) with a standard deviation of 2.9in (7cm) when using only a single camera match. When using three camera matches, the average placement from known locations was 2.4in (6cm) with a standard deviation of 1.1in (3cm). This results in an average improvement of 56.3% in location accuracy when using three camera matches over one camera match (Figures 8-11, Table 2).

Vehicle orientation (yaw, pitch, and roll) for site one was found to be within .5° of known orientations on average, with a standard deviation of .1° with a single camera match. Orientations found with three camera matches were found to FIGURE 8 Evidence placements (spray chalk and vehicle location) for site 1 using only 1 camera match. Red coloring represents the know evidence locations.

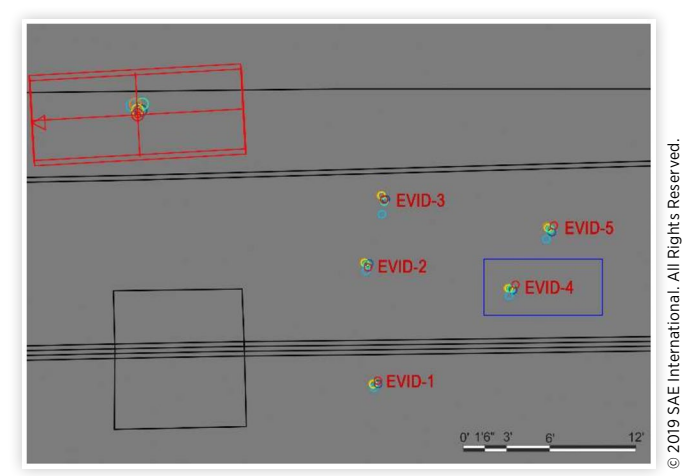


FIGURE 9 A zoomed in area of blue box from Figure 8 showing placements of evidence #4 using a single camera match. Red coloring represents the know evidence locations.

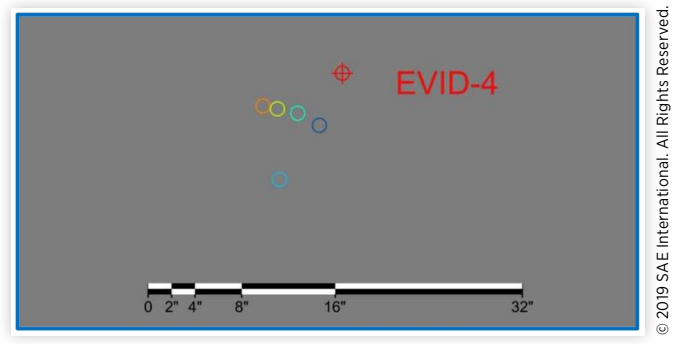


FIGURE 10 Evidence placements (spray chalk and vehicle location) for site 1 using 3 camera matches. Red coloring represents the known evidence locations.

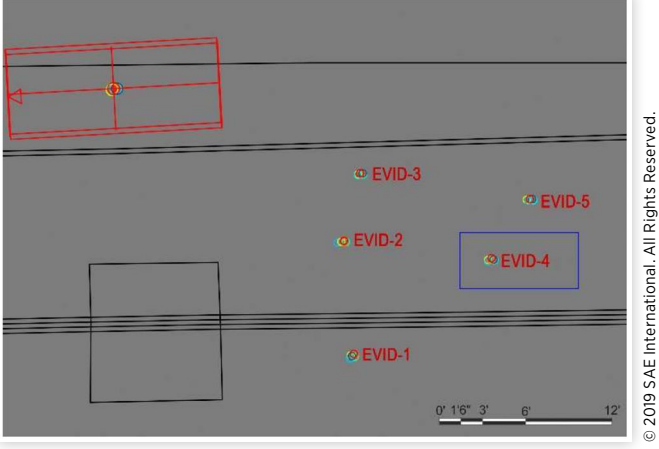
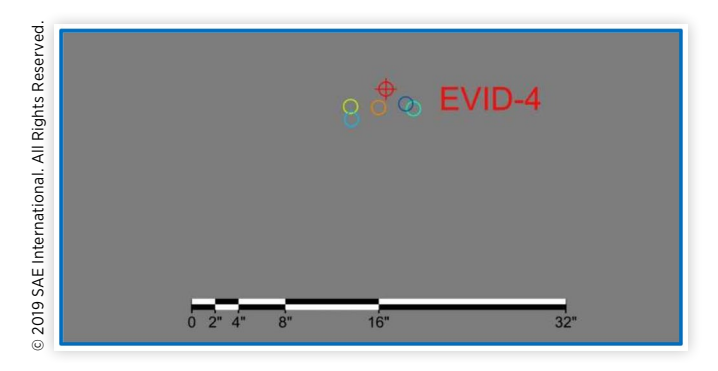
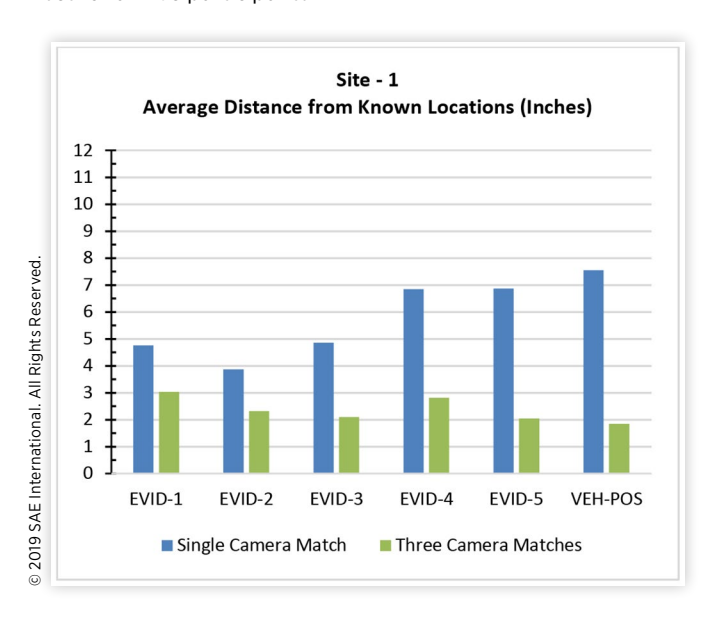


FIGURE 11 A zoomed in area of blue box from Figure 10 showing placements of evidence #4 using 3 camera matches. Red coloring represents the know evidence locations.



**TABLE 2** Average distances for evidence locations (spray chalk and vehicle position) from known locations including the single camera match data set and the three camera match data set for all five participants.



be within .4° of known orientations on average, with a standard deviation of .2°.

## Site-02: LiDAR Comparison

To evaluate the accuracy of the USGS LiDAR in comparison to traditionally collected LiDAR or ground-based LiDAR, a distance comparison was performed. For this comparison, a section of overlapping data from both the USGS LiDAR and the ground-based LiDAR was chosen. This section had a calculated area of 2496ft<sup>2</sup> (232m<sup>2</sup>) (Figure 12).

Within the selected area the ground-based LiDAR data contained 885,053 points for a resolution of approximately 355 points ft<sup>2</sup> (3,816 points m<sup>2</sup>). The USGS LiDAR data contained 1,566 points for a resolution of approximately 0.6 ft<sup>2</sup> (6.8 points m<sup>2</sup>). The distance comparison was performed in CloudCompare [37] using the compute cloud distance tool. This tool evaluates the distance between points of one 3D point cloud to another based on the a nearest neighbor.

**FIGURE 12** Orthographic top view of site 2 showing the area used for terrain comparison. The grayscale area represents the ground-based LiDAR point cloud, the red and orange colored points represent the USGS LiDAR outside of the comparison area. The USGS LiDAR points that were used in comparison are colorized based on distance away from the ground-based LiDAR data set (Distances by color shown in <u>Table 3</u>).

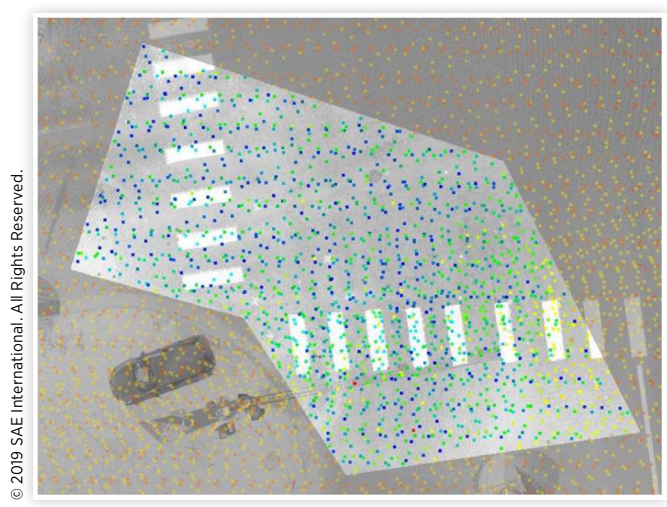
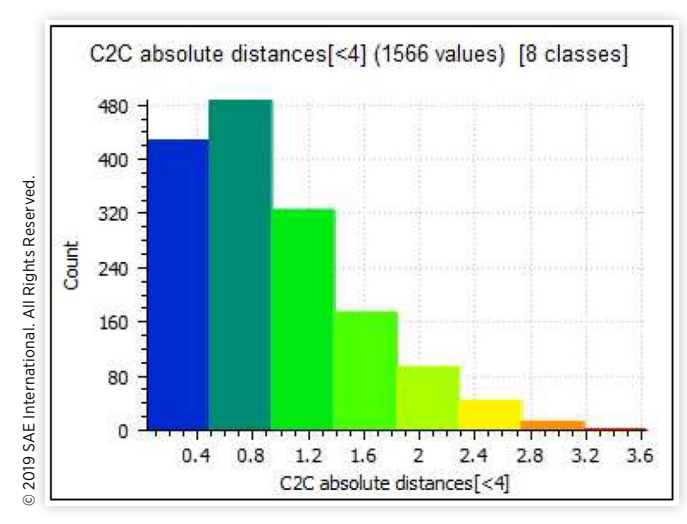


**TABLE 3** A histogram showing USGS LiDAR point cloud distances (inches) from ground-based LiDAR points.



All distance measurements include both horizontal and vertical distances between the two point clouds. When the USGS point cloud and the ground-based point clouds were compared, approximately 58% of the points were found to be within 0.9in, approximately 79% of the points were found to be within 1.4in, and approximately 90% of the points were found to be within 1.8in (Table 3).

#### Site-02: Photogrammetry

The second site, an urban business area, had the most accurate results. The average distance for placing the spray chalk marks

and for the center location of the vehicle from known locations for all five participants was 4.4in (11cm) with a standard deviation of 2.8in (7cm) when using only a single camera match. When using three camera matches, the average placement from known locations was 1.3in (3cm) with a standard deviation of 0.5in (1cm). This results in an average improvement of 67.8% in location accuracy when using three camera matches over one camera match (Figures 13-16, Table 4).

Vehicle orientation (yaw, pitch, and roll) for site two was found to be within .5° of known orientations on average, with a standard deviation of .1° with a single camera match. Orientations found with three camera matches were found to be within .4° of known orientations on average, with a standard deviation of .2°.

#### Site-03: LiDAR Comparison

To evaluate the accuracy of the USGS LiDAR in comparison to traditionally collected LiDAR or ground-based LiDAR, a distance comparison was performed. For this comparison,

**FIGURE 13** Evidence placements (spray chalk and vehicle location) for site 2 using only 1 camera match. Red coloring represents the known evidence locations.

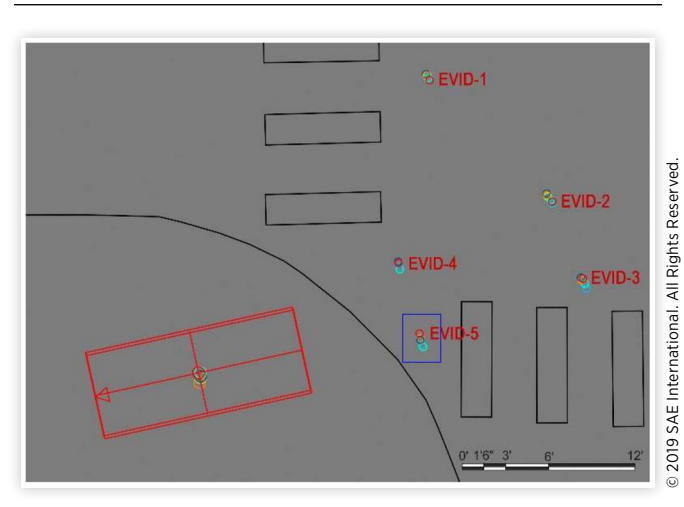


**FIGURE 14** A zoomed in area of blue box from Figure 13 showing placements of evidence #5 using a single camera match. Red coloring represents the know evidence locations.



FIGURE 15 Evidence placements (spray chalk and vehicle location) for site 2 using 3 camera matches. Red coloring represents the known evidence locations.

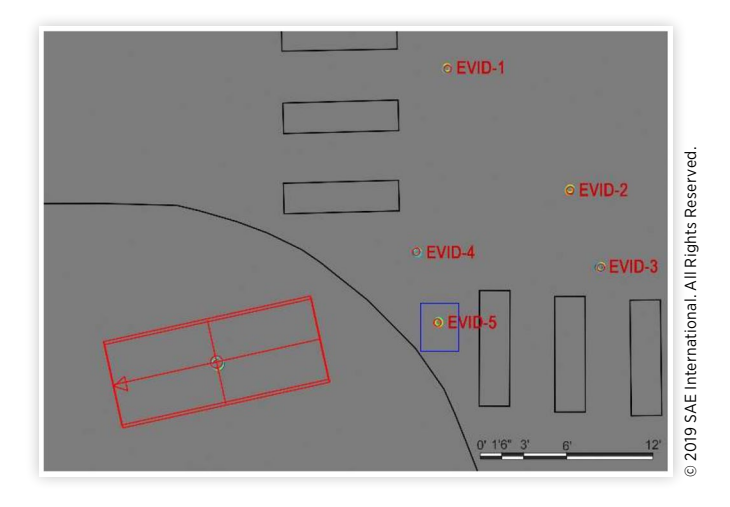
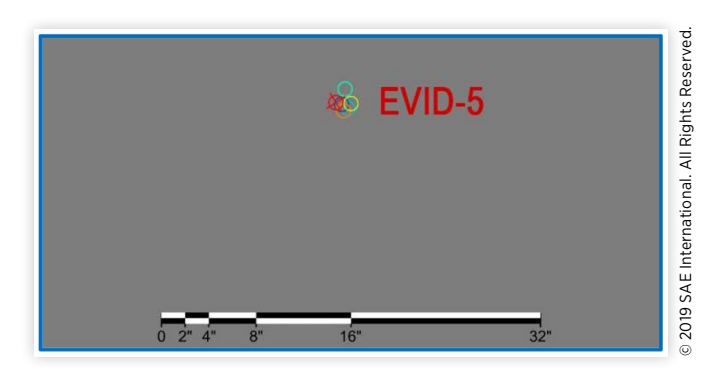
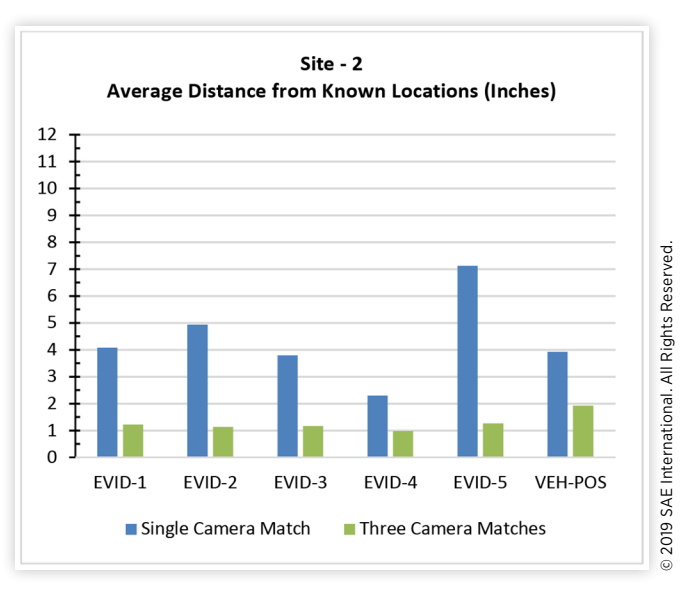


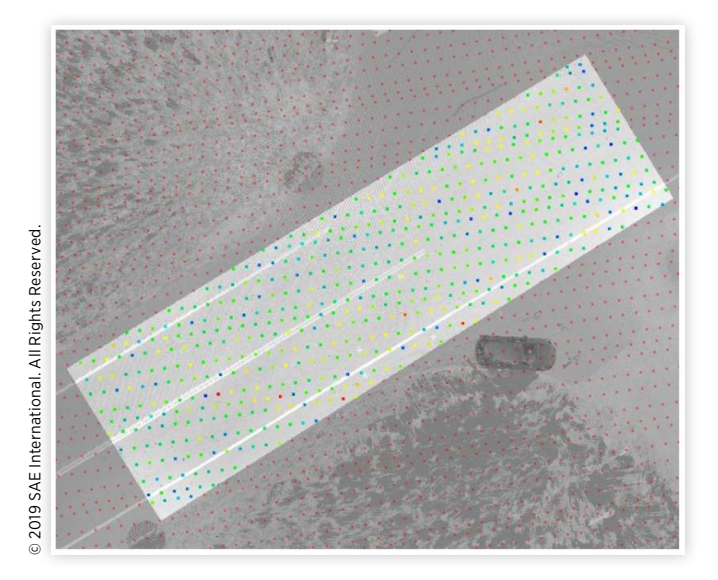
FIGURE 16 A zoomed in area of blue box from Figure 15 showing placements of evidence #5 using 3 camera matches. Red coloring represents the know evidence locations.



**TABLE 4** Average distances for evidence locations (spray chalk and vehicle position) from known locations including the single camera match data set and the three camera match data set for all five participants.



**FIGURE 17** Orthographic top view of site 2 showing the area used for terrain comparison. The grayscale area represents the ground-based LiDAR point cloud, the red colored points represent the USGS LiDAR outside of the comparison area. The USGS LiDAR points that were used in comparison are colorized based on distance away from the ground-based LiDAR data set (Distances by color shown in Table 3).



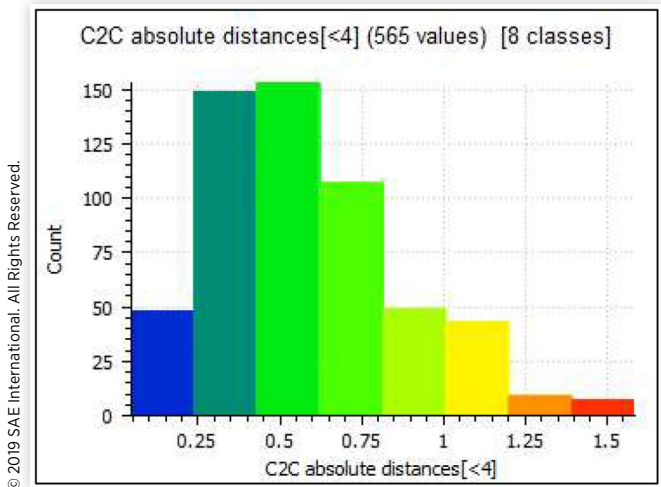
a section of overlapping data from both the USGS LiDAR and the ground-based LiDAR was chosen. This section was approximately 96ft (29m) long and 34ft (10m) wide (Figure 17).

Within the selected area the ground-based LiDAR data contained 1,140,542 points for a resolution of approximately 331 points ft² (3,568 points m²). The USGS LiDAR data contained 565 points for a resolution of approximately 0.2 ft² (1.8 points m²). The distance comparison was performed in CloudCompare [37] using the compute cloud distance tool. This tool evaluates the distance between points of one 3D point cloud to another based on the a nearest neighbor. All distance measurements include both horizontal and vertical distances between the two point clouds. When the USGS point cloud and the ground-based point clouds were compared, approximately 62% of the points were found to be within 0.6in, approximately 81% of the points were found to be within 0.8in, and approximately 97% of the points were found to be within 1.2in (Table 5).

#### Site-03: Photogrammetry

The third site which was more rural in nature and located inside of a state park, had the least accurate results. The average distance for placing the spray chalk marks and for the center location of the vehicle from known locations for all five participants was 7.4in (19cm) with a standard deviation of 4.1in (10cm) when using only a single camera match. When using three camera matches, the average placement from known locations was 5.3in (14cm) with a standard deviation of 2.7in (7cm). This results in an average improvement of 26.9%

**TABLE 5** A histogram showing USGS LiDAR point cloud distances (inches) from ground-based LiDAR points.



in location accuracy when using three camera matches over one camera match (<u>Figures 18-21</u>, <u>Table 6</u>).

Vehicle orientation (yaw, pitch, and roll) for site three was found to be within .4° of known orientations on average, with a standard deviation of .3° with a single camera match. Orientations found with three camera matches were found to be within .2° of known orientations on average, with a standard deviation of .1°.

## One Camera Match and Three Camera Matches

With a single camera match the combined average distances from all three sites from placed evidence (spray chalk and vehicle) to known locations was found on average to be 5.8in (15cm) from known locations, with a standard deviation of 1.2in (3cm). And the combined average vehicle orientation

FIGURE 18 Evidence placements (spray chalk and vehicle location) for site 3 using only 1 camera match. Red coloring represents the known evidence locations.

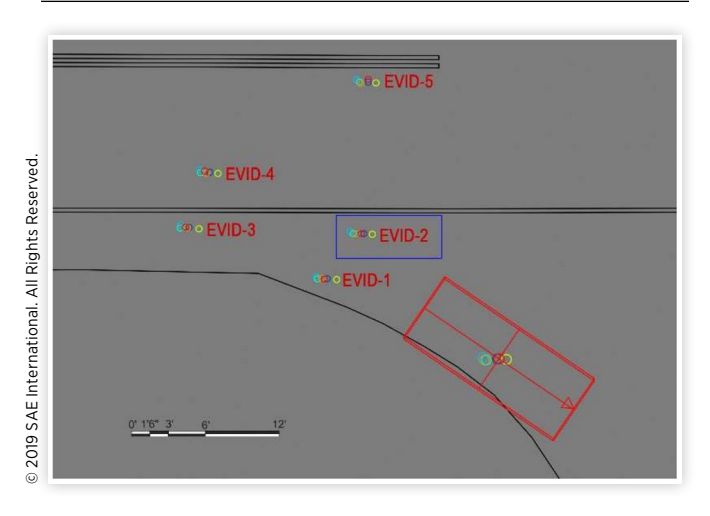
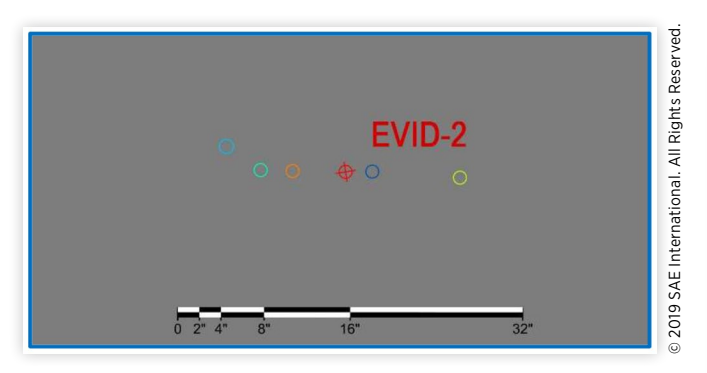


FIGURE 19 A zoomed in area of blue box from Figure 18 showing placements of evidence #2 using a single camera match. Red coloring represents the know evidence locations.



**FIGURE 20** Evidence placements (spray chalk and vehicle location) for site 3 using 3 camera matches. Red coloring represents the known evidence locations.

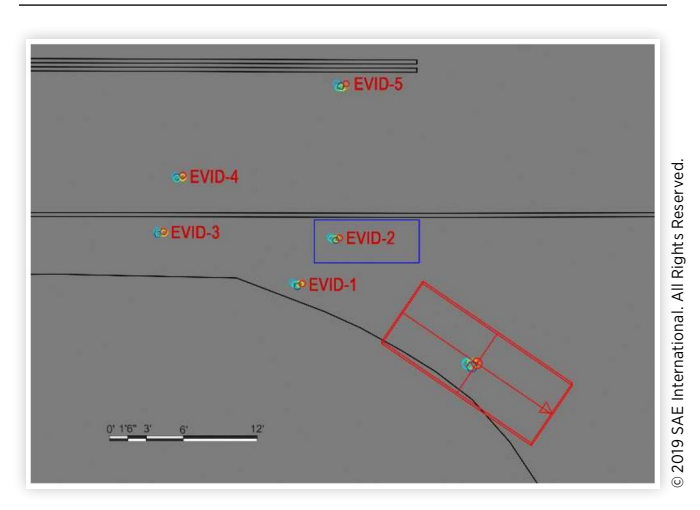
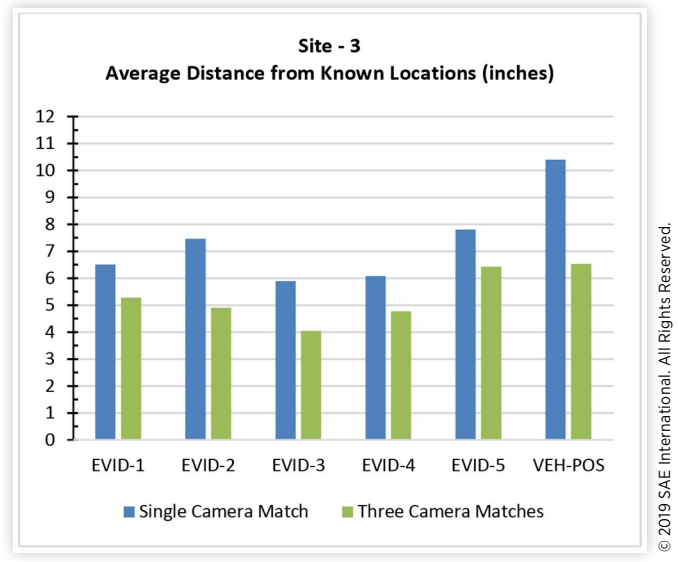


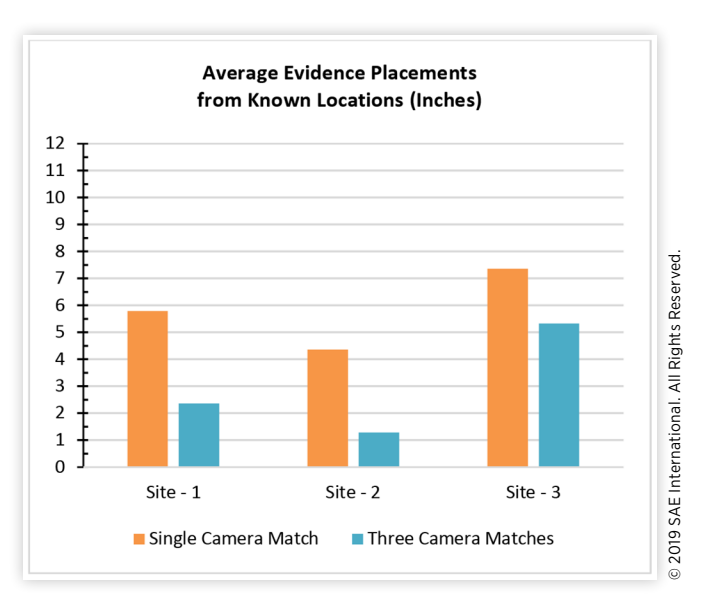
FIGURE 21 A zoomed in area of blue box from Figure 20 showing placements of evidence #2 using 3 camera matches. Red coloring represents the know evidence locations.



**TABLE 6** Average distances for evidence locations (spray chalk and vehicle position) from known locations including the single camera match data set and the three camera match data set for all five participants.



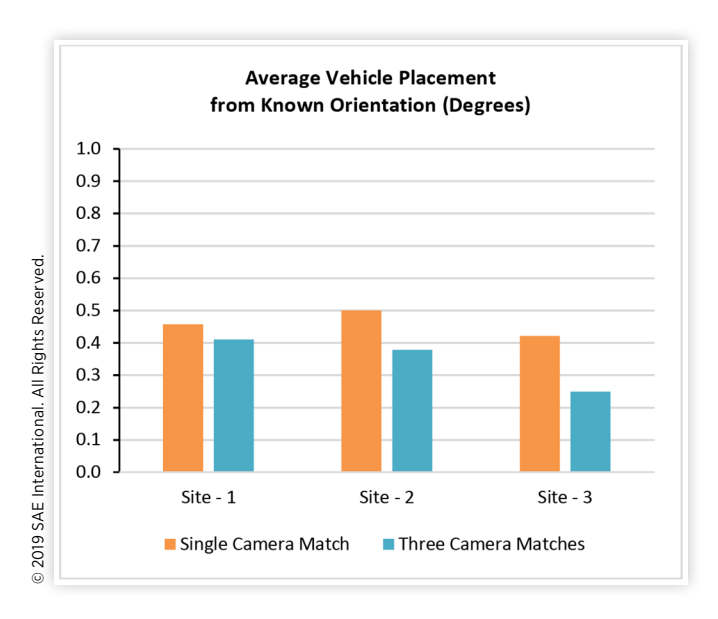
**TABLE 7** Average distance from evidence placements to know evidence locations for all three sites using only one camera match.



differences on all axes for all three sites was found to be  $0.5^{\circ}$  with a standard deviation of  $0.03^{\circ}$  (<u>Tables 7, 8</u>).

With three camera matches the combined average distances from all three sites from placed evidence (spray chalk and vehicle) to known locations was found on average to be 3.0in (8cm) from known locations, with a standard

**TABLE 8** Average distance from evidence placements to know evidence locations for all three sites using three camera matches



deviation of 1.7in (4cm). And the combined average vehicle orientation differences on all axes for all three sites was found to be 0.3° with a standard deviation of 0.07° (<u>Tables 7, 8</u>).

## **Summary/Conclusions**

Based on the results achieved through this study, the authors believe that this methodology will prove useful to the accident reconstruction community. While more accurate results may be achieved with a site visit, there are instances where a site visit is impractical or of little value due to significant site changes. In these instances, using USGS LiDAR, aerial photographs, and photos containing evidence to create a 3D model may be the best if not only solution available.

On average, placement of evidence using three camera matches was shown to have a 50.3% improvement in evidence placement over using only one camera match. The first site showed a 56.3% improvement, the second site showed a 67.8% improvement and the third site showed a 50.3% improvement. Consistent with previous literature, highly accurate solutions can be achieved with a single camera match, provided that there is a known surface, but in general, including additional camera matches with unique vantages to the photogrammetry solution, has been shown to increase accuracy.

### Limitations

There are potential limitations when using this methodology. Aerial imagery must be available with a resolution high enough to uniquely distinguish features to be used in camera matching. Aerial images can contain perspective distortion based on the incidence angle of the camera when the photograph was taken. This distortion is prevalent in scenes with

significant elevational differences and particularly over larger distances. The USGS LiDAR data sets are not imagery based and are therefore not subject to perspective distortion. Inability to align an aerial with USGS LiDAR can be an indicator of perspective distortion. The alignment can be used as a method for evaluating if perspective distortion is present within an aerial image.

Similarly, USGS LiDAR must be available. While untested, it may be possible to achieve similar results with lower resolution USGS LiDAR point clouds. However, as the 3DEP program progresses, higher resolution will become available throughout the United States.

This study represents a less than ideal situation for obtaining evidence from photographs using camera matching photogrammetry without a site visit. With a site visit and opportunity to document a site using traditional means, smaller differences between placed evidence locations and known evidence locations can be achieved.

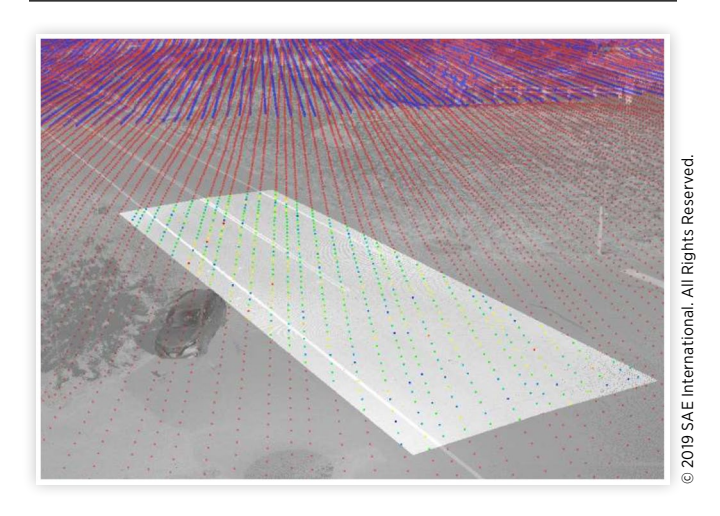
The accuracy of the camera matching process is dependent on the angle of incidence as determined by the elevation of the camera, the elevation of the evidence to be placed, and the distance between the camera and the evidence [14]. Similarly, lower resolution imagery can also limit the photogrammetric accuracy achievable. Lens distortion can also affect photogrammetric accuracy. The accuracy of evidence placement within this paper may not be achievable when lens distortion is not considered and when appropriate measures for lens correction are not implemented [41, 42, 43].

#### **Discussion**

While all three sites were classified as having the same LiDAR point cloud resolution from USGS (0.350001 to 0.700000m²), the calculated points per square meter from the comparison area of site 3 fell below this resolution. The authors noticed that within the USGS data sets there are what appears to be overlapping of LiDAR data. This is likely from multiple passes and collected for alignment purposes. This can be seen within the LiDAR data downloaded for site 3, but not in the area where the USGS LiDAR point cloud was compared to the ground-based LiDAR point cloud. The higher density data in this set was used in the camera matching process that utilized data beyond the LiDAR comparison area, but the lower resolution comparison data was used for creating the surfaced terrain for tracing camera match evidence (Figure 22).

The National Center for Airborne Laser Mapping (NCALM) is another online resource for Aerial LiDAR [44]. While the data does not appear to have intensity values, this is another potential resource for reconstructing scenes using historical LiDAR data. The data collection is funded by private investors and typically released to the public six months to two years afterwards depending on the data policy type, and perhaps sooner if approved by the investor. The data is then released through OpenTopography [45].

While all of the vehicle orientations were found to be within 0.5°, on average the pitch was found to be the most accurate axis. The authors believe and attribute this to the ability to distinguish small differences in angles more easily **FIGURE 22** Perspective view of site 3 showing the area used for terrain comparison and the higher resolution data in the distance (dark blue). The grayscale area represents the ground-based LiDAR point cloud, the red and blue colored points represent the USGS LiDAR outside of the comparison area. The USGS LiDAR points that were used in comparison are colorized based on distance away from the ground-based LiDAR data set (Distances by color shown in <u>Table 5</u>).



over greater distances. The overall vehicle length is greater than the its overall width or height, making it easier to distinguish the axis or axes along which the length of the vehicle corresponds. With photographs taken near eye level like those in this study, small changes in the vehicle pitch would be most easily distinguished, allowing for the pitch angle to be orientated with greater accuracy. In instances where photographs or video was taken from a more aerial vantage, the vehicle yaw angle would be more easily distinguished allowing for placement in this axis with greater accuracy.

It is worth noting that photogrammetry is a science. There is no error inherent with photogrammetry, including camera-match photogrammetry. Photogrammetry errors are introduced when there is a lack of accurate useable data, a misunderstanding of the processes required for accurate photogrammetry solutions, misuse of software, the acceptance of inaccurate, lower quality, or less than perfect solutions, or any combination of these.

Camera matching photogrammetry was performed using Autodesk 3ds Max 2017. Future updates to this software and use of other software with more automated camera solutions may further improve upon these results. Likewise, higher resolution USGS LiDAR data and newer data with improved filtering models may also improve upon these results.

### References

- Fenton, S. and Kerr, R., "Accident Scene Diagramming Using New Photogrammetric Technique," SAE Technical Paper 970944, 1997, doi:10.4271/970944.
- 2. Neale, W., Fenton, S., McFadden, S., and Rose, N., "A Video Tracking Photogrammetry Technique to Survey Roadways

- for Accident Reconstruction," SAE Technical Paper <u>2004-01-1221</u>, 2004, doi:<u>10.4271/2004-01-1221</u>.
- Day, T. and Hargens, R., "A Personal Computer Program for Drawing Accident Sites," SAE Technical Paper <u>880068</u>, 1988, doi:<u>10.4271/880068</u>.
- Coleman, C., Tandy, D., Colborn, J., and Ault, N., "Applying Camera Matching Methods to Laser Scanned Three Dimensional Scene Data with Comparisons to Other Methods," SAE Technical Paper <u>2015-01-1416</u>, 2015, doi:10.4271/2015-01-1416.
- Rudny, D. and Sallmann, D., "The Use of Electronic Survey Equipment in the Creation of Accident Scene Diagrams," SAE Technical Paper 950361, 1995, doi:10.4271/950361.
- Campbell, A. and Friedrich, R., "Adapting Three-Dimensional Animation Software for Photogrammetry Calculations," SAE Technical Paper 930904, 1993, doi:10.4271/930904.
- Callahan, M., LeBlanc, B., Vreeland, R., and Bretting, G., "Close-Range Photogrammetry with Laser Scan Point Clouds," SAE Technical Paper <u>2012-01-0607</u>, 2012, doi:10.4271/2012-01-0607.
- 8. Terpstra, T., Beier, S., and Neale, W., "The Application of Augment Reality to Reverse Camera Projection," SAE Technical Paper 2019-01-0424, 2019.
- 9. Bailey, A., Funk, J., Lessley, D., Sherwood, C. et al., "Validation of a Videogrammetry Technique for Analyzing American Football Helmet Kinematics," *Sports Biomechanics* 1-23, 2018, doi:10.1080/14763141.2018.1513059.
- Dilich, M. and Goebelbecker, J., "Accident Investigation and Reconstruction Mapping with Aerial Photography," SAE Technical Paper 960894, 1996, doi:10.4271/960894.
- 11. Jensen, J.R., Remote Sensing of the Environment: An Earth Resource Perspective (Harlow: Pearson, 2013).
- Lillesand, T.M., Kiefer, R.W., and Chipman, J.W., Remote Sensing and Image Interpretation (New York: Wiley, 1999).
- 13. "What Is 3DEP?" 3D Elevation Program, <a href="https://www.usgs.gov/core-science-systems/ngp/3dep">https://www.usgs.gov/core-science-systems/ngp/3dep</a>, accessed Oct. 9, 2018.
- 14. Terpstra, T., Dickinson, J., and Hashemian, A., "Using Multiple Photographs and USGS LiDAR to Improve Photogrammetric Accuracy," *SAE Int. J. Trans. Safety* 6(3), 2018, doi:10.4271/2018-01-0516.
- Woolley, R., White, K., Asay, A., and Bready, J.,
  "Determination of Vehicle Crush from Two Photographs and the Use of 3D Displacement Vectors in Accident Reconstruction," SAE Technical Paper <u>910118</u>, 1991, doi:10.4271/910118.
- 16. Wester-Ebbinghaus, W. and Wezel, U., "Photogrammetric Deformation Measurement of Crash Vehicles," SAE Technical Paper 860207, 1986, doi:10.4271/860207.
- Gillen, L., "Photogrammetric Mapping of Vehicle Deformations," SAE Technical Paper <u>861421</u>, 1986, doi:10.4271/861421.
- 18. Fenton, S., Neale, W., Rose, N., and Hughes, C., "Determining Crash Data Using Camera Matching Photogrammetric Technique," SAE Technical Paper 2001-01-3313, 2001, doi:10.4271/2001-01-3313.
- Rentschler, W. and Uffenkamp, V., "Digital Photogrammetry in Analysis of Crash Tests," SAE Technical Paper <u>1999-01-</u> 0081, 1999, doi:10.4271/1999-01-0081.

- Behring, D., Thesing, J., Becker, H., and Zobel, R., "Optical Coordinate Measuring Techniques for the Determination and Visualization of 3D Displacements in Crash Investigations," SAE Technical Paper <u>2003-01-0891</u>, 2003, doi:10.4271/2003-01-0891.
- O'Shields, L., Kress, T., Hungerford, J., and Aikens, C.,
  "Determination and Verification of Equivalent Barrier Speeds (EBS) Using PhotoModeler as a Measurement Tool," SAE Technical Paper 2004-01-1208, 2004, doi:10.4271/2004-01-1208.
- 22. Rose, N., Neale, W., Fenton, S., Hessel, D. et al., "A Method to Quantify Vehicle Dynamics and Deformation for Vehicle Rollover Tests Using Camera-Matching Video Analysis," *SAE Int. J. Passeng. Cars Mech. Syst.* 1(1):301-317, 2009, doi:10.4271/2008-01-0350.
- 23. Rucoba, R., Duran, A., Carr, L., and Erdeljac, D., "A Three-Dimensional Crush Measurement Methodology Using Two-Dimensional Photographs," SAE Technical Paper 2008-01-0163, 2008, doi:10.4271/2008-01-0163.
- 24. Chou, C., McCoy, R., Le, J., Fenton, S. et al., "Image Analysis of Rollover Crash Tests Using Photogrammetry," SAE Technical Paper 2006-01-0723, 2006, doi:10.4271/2006-01-0723.
- Rose, N., Neale, W., Fenton, S., Hessel, D. et al., "A Method to Quantify Vehicle Dynamics and Deformation for Vehicle Rollover Tests Using Camera-Matching Video Analysis," SAE Int. J. Passeng. Cars - Mech. Syst. 1(1):301-317, 2009, doi:10.4271/2008-01-0350.
- Peck, L. and Cheng, M., "The Accuracy of an Optimized, Practical Close-Range Photogrammetry Method for Vehicular Modeling," SAE Int. J. Trans. Safety 4(2):245-266, 2016, doi:10.4271/2016-01-1462.
- 27. Massa, D., "Using Computer Reverse Projection Photogrammetry to Analyze an Animation," SAE Technical Paper 1999-01-0093, 1999, doi:10.4271/1999-01-0093.
- 28. Alden, A., Mayer, B., Mcgowen, P., Sherony, R. et al., "Animal-Vehicle Encounter Naturalistic Driving Data Collection and Photogrammetric Analysis," SAE Technical Paper 2016-01-0124, 2016, doi:10.4271/2016-01-0124.
- 29. Neale, W., Hessel, D., and Koch, D., "Determining Position and Speed through Pixel Tracking and 2D Coordinate Transformation in a 3D Environment," SAE Technical Paper 2016-01-1478, 2016, doi:10.4271/2016-01-1478.
- Neale, W., Marr, J., and Hessel, D., "Nighttime Videographic Projection Mapping to Generate Photo-Realistic Simulation Environments," SAE Technical Paper <u>2016-01-1415</u>, 2016, doi:10.4271/2016-01-1415.
- 31. Neale, W., Marr, J., and Hessel, D., "Video Projection Mapping Photogrammetry through Video Tracking," SAE Technical Paper 2013-01-0788, 2013, doi:10.4271/2013-01-0788.
- 32. Grimes, C., Roescher, T., Suway, J., and Welcher, J., "Comparing the Accuracy of Image Based Scanning Techniques to Laser Scanners," SAE Technical Paper <u>2018-01-0525</u>, 2018, doi:10.4271/2018-01-0525.
- Terpstra, T., Voitel, T., and Hashemian, A., "A Survey of Multi-View Photogrammetry Software for Documenting Vehicle Crush," SAE Technical Paper <u>2016-01-1475</u>, 2016, doi:10.4271/2016-01-1475.
- 34. Luhmann, T., Stuart, R., Stephen, K., and Jan, B., *Close-Range Photogrammetry and 3D Imaging* 2nd Edition (Walter De Gruyter GmbH, 2014).

- 35. Jurkofsky, D., "Accuracy of SUAS Photogrammetry for Use in Accident Scene Diagramming," *SAE Int. J. Trans. Safety* 3(2):136-152, 2015, doi:10.4271/2015-01-1426.
- 36. Carter, N., Hashemian, A., Rose, N., and Neale, W., "Evaluation of the Accuracy of Image Based Scanning as a Basis for Photogrammetric Reconstruction of Physical Evidence," SAE Technical Paper 2016-01-1467, 2016, doi:10.4271/2016-01-1467.
- 37. CloudCompare (version 2.9 Beta) [GPL Software]. <a href="http://www.danielgm.net/cc/">http://www.danielgm.net/cc/</a>
- U.S. Department of the Interior, U.S. Geological Survey, Collection and Delineation of Spatial Data, "Chapter 4: Lidar Base Specification, Version 1.2" National Geospatial Program, 2014.
- 39. Itoosoft. "Free Plugins; ColorEdge, Glue, Clone." IToo Software. Accessed Oct. 11, 2018. <a href="https://www.itoosoft.com/freeplugins/glue">https://www.itoosoft.com/freeplugins/glue</a>.
- 40. Maune, D.F., and Nayegandhi A.. *Digital Elevation Model Technologies and Applications*, The DEM Users Manual, Third Edition. Maryland: Selbstverl, Der American Society for Photogrammetry and Remote Sensing, 2018.
- 41. Neale, W., Hessel, D., and Terpstra, T., "Photogrammetric Measurement Error Associated with Lens Distortion," SAE Technical Paper 2011-01-0286, 2011, doi:10.4271/2011-01-0286.
- 42. Wolfgang, H "Correcting Lens Distortions in Digital Photographs" <a href="https://www.imagemagick.org/Usage/lens/correcting\_lens\_distortions.pdf">https://www.imagemagick.org/Usage/lens/correcting\_lens\_distortions.pdf</a>.
- Terpstra, T., Miller, S., and Hashemian, A., "An Evaluation of Two Methodologies for Lens Distortion Removal when EXIF Data Is Unavailable," SAE Technical Paper <u>2017-01-1422</u>, 2017, doi:10.4271/2017-01-1422.
- 44. "Home," Home, OpenTopography, Dec. 20, 2018, <a href="https://opentopography.org/">https://opentopography.org/</a>, accessed Jan. 15, 2019.
- "NCALM," Welcome, NCALM, <a href="http://ncalm.cive.uh.edu/">http://ncalm.cive.uh.edu/</a>, accessed Jan. 15, 2019.

#### **Contact Information**

#### **Toby Terpstra**

Kineticorp, LLC (303) 733-1888 tterpstra@kineticorp.com www.kineticorp.com

### Acknowledgments

The authors wish to thank Steven Beier and David Hessel for their general assistance and specifically for their time spent performing camera matching photogrammetry.

#### **Definitions/Abbreviations**

3DEP - Three-Dimensional Elevation Program

**ASPRS** - American Society of Photogrammetry and Remote Sensing

**camera matching** - A close-range photogrammetry method where known 3D models are aligned to a photograph within

computer driven software. The software is utilized to solve for the camera location, orientation, and field of view.

**EXIF** - Exchangeable image file format, metadata stored within photographs, videos, and audio files

**LAS** - LASer public file format developed by the ASPRS for 3D point cloud data exchange

**LiDAR** - Portmanteau for light and radar, or an acronym for Light Detection and Ranging

NCALM - National Center for Airborne Laser Mapping

**photo scanning** - A photogrammetric application where multiple (typically many) photographs with significant overlap in subject matter, are imported into software that solves for each camera location and creates a resulting 3D point cloud (also referred to as Multi-view photogrammetry)

**photogrammetry** - Defined by ASPRS as: The art, science, and technology of obtaining reliable information about physical objects and the environment through process of recording, measuring and interpreting photographic images and patterns of recorded radiant electromagnetic energy and other phenomena.

**point cloud** - Large numbers (typically millions) of 3D data points commonly obtained through 3D scanning or photo scanning

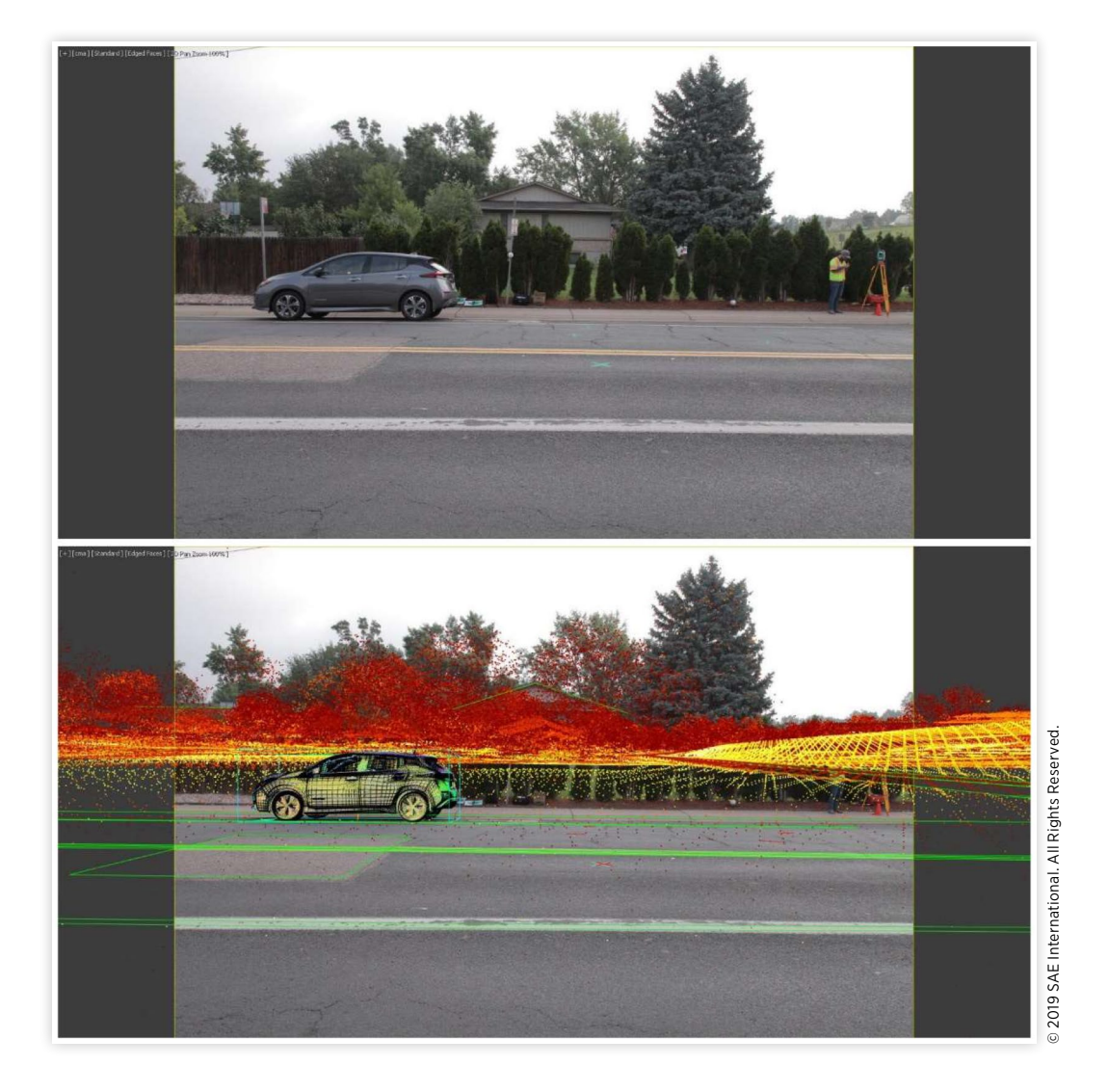
POR - Point of Rest

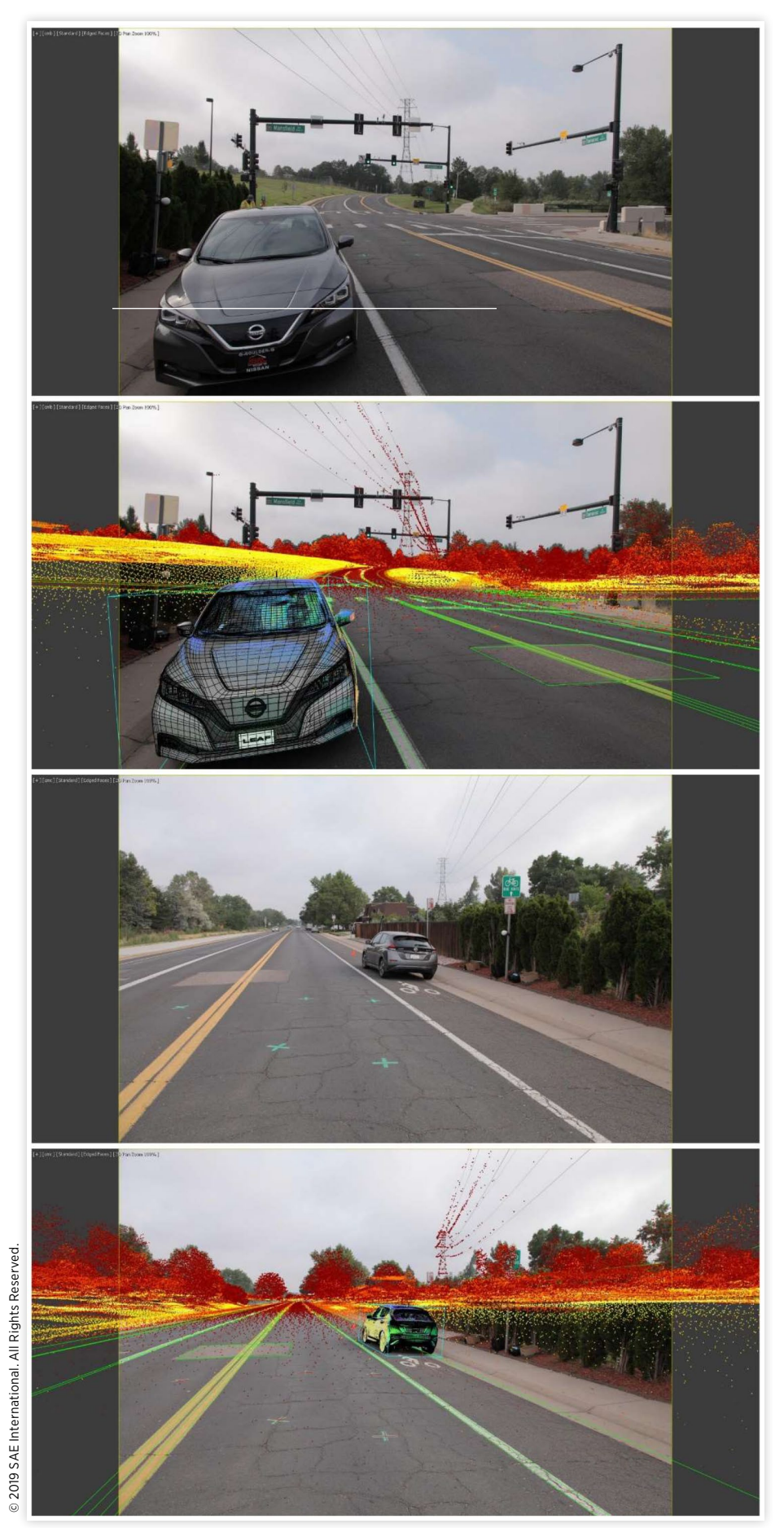
SOR - Statistical Outlier Removal

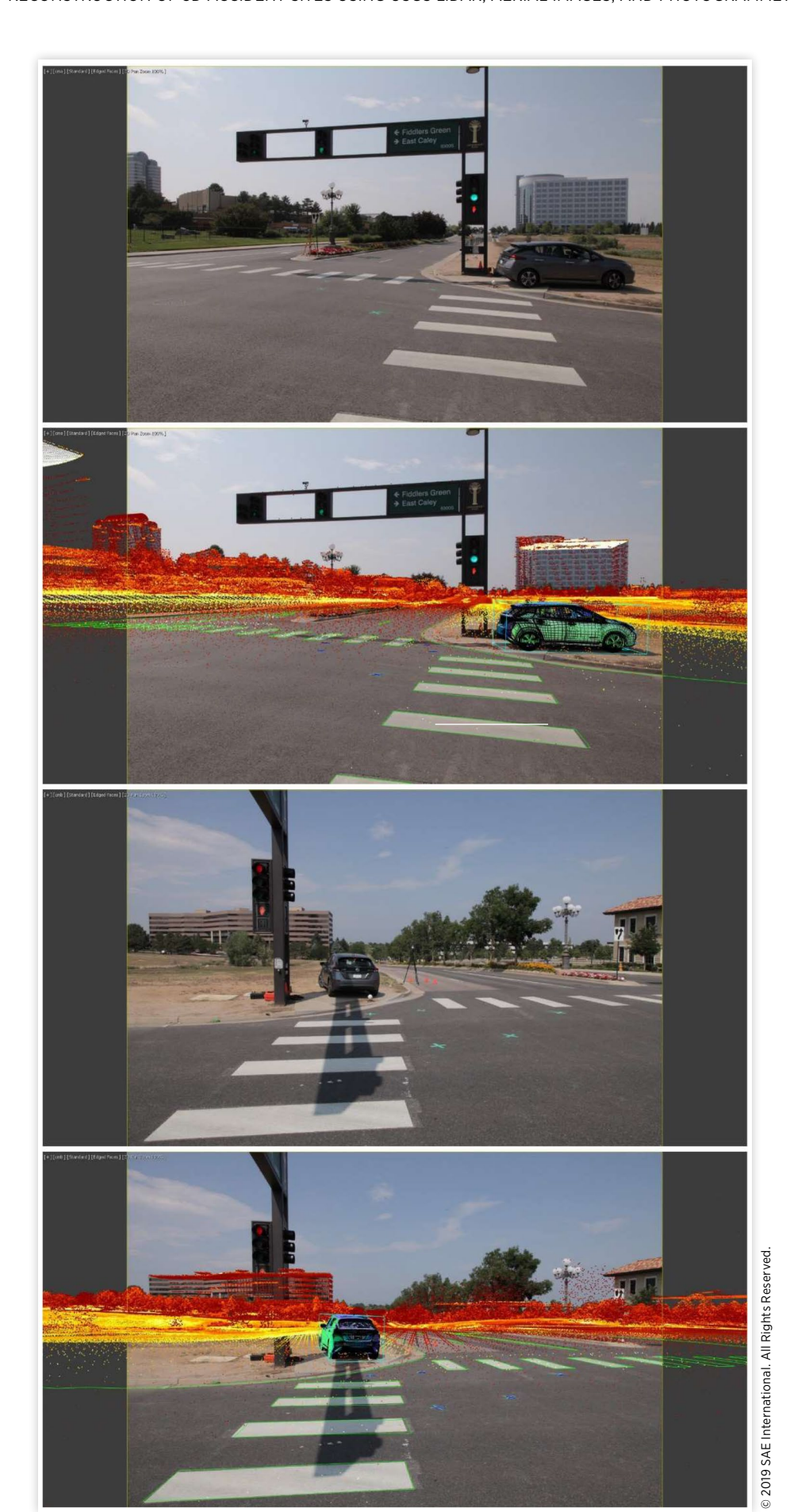
**USGS** - United States Geological Survey

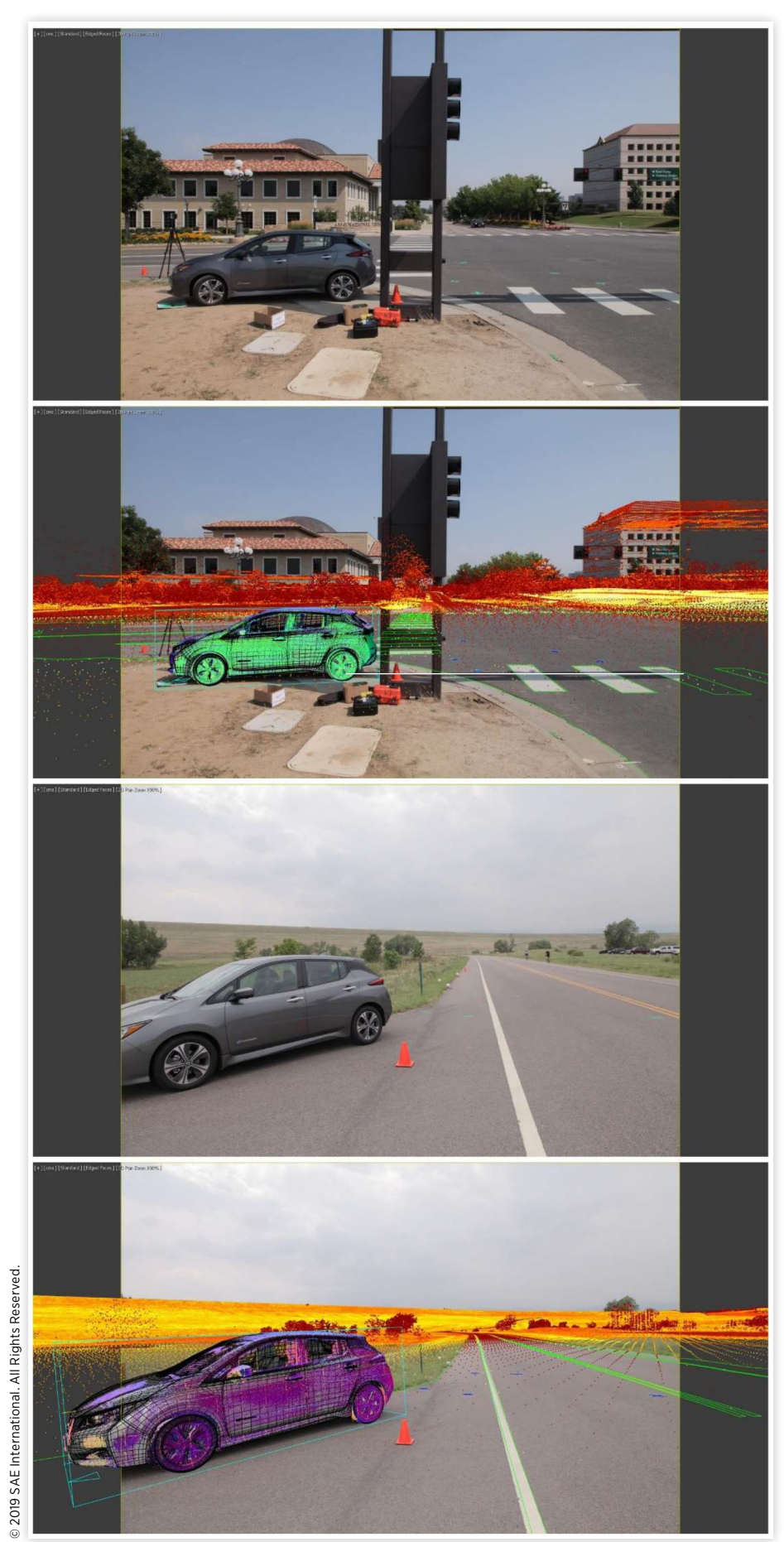
## **Appendix A**

Camera matches from one of the five participants including all three camera matches from each of the three sites.











## **Appendix B**

© 2019 SAE International. All Rights Reserved.

Recorded known evidence locations and evidence placements from all 5 participants at all three sites.

Site 1: Known evidence locations EVID-1 -437.36 53.45 5941.00 -318.71 -244.09 5940.30 VEH-POS -397.07 349.11 5963.40 Site 1: Evidence placements (one camera match) Dif Dif Dif EVID-1 -442.02 55.32 5940.72 -442.24 54.35 5940.88 -441.43 54.95 5940.61 -443.73 51.9923 5940.61 6.55 -439.39 51.39 5940.94 2.88 5.02 4.96 4.36 EVID-2 -369.48 125.64 -369.37 5940.43 -367.33 5940.03 5939.95 124.73 5940.06 -369.76 122.44 -373.64 119.753 5940.46 121.67 5.47 4.61 2.30 3.30 3.62 EVID-3 -317.89 -317.55 5938.56 5939.26 5938.59 150.86 5938.42 4.66 150.12 4.01 -319.85 145.34 5939.26 1.56 -329.21 139.971 -317.51 145.51 1.72 12.31 EVID-4 -308.84 5940.98 -308.23 5941.12 5941.32 5941.35 -306.99 5941.12 20.33 19.23 -307.39 17.66 -312.7 15.221 15.58 7.37 5.12 10.51 4.87 6.35 EVID-5 -248.57 28.28 5939.92 6.07 -248.73 26.60 5940.08 5.22 -248.39 24.68 5940.61 4.33 -256.75 21.7278 5940.6 12.90 -249.42 21.93 5940.13 5.79 VEH-POS -391.39 5962.82 9.28 5962.48 4.01 5962.26 10.06 -394.05 5961.47 9.44 356.42 -394.17 -387.45 357.842 -392.53 351.73 351.81 349.18 AVG (in) 6.31 AVG (in) 4.86 AVG (in) AVG (in) 9.17 AVG (in) 3.97 AVG (cm) AVG (cm) 12.34 AVG (cm) 11.74 AVG (cm) 23.29 AVG (cm) 10.10 VEH-ROT 132.48 Site 1: Evidence placements (three camera matches) Dif х Υ Z х Z х Υ Z х Υ Z х Υ EVID-1 437.96 51.44 5940.78 2.10 -439.99 54.53 5940.62 2.87 -438.98 51.18 5940.95 2.79 -442.33 53.38 5940.61 4.98 -439.79 53.44 5941.11 2.43 5940.74 5940.41 5941.37 EVID-2 -371.18 119.45 5941.39 -372.64 121.64 5941.04 -370.29 118.46 -375.09 123.58 -370.59 120.20 1.19 2.47 2.03 5.63 0.27 EVID-3 5939.20 5938.82 5939.65 -318.91 145.46 5939.38 0.95 -320.69 147.05 2.10 -318.21 143.88 -321.45 146.70 5939.24 -317.53 144.78 2.01 EVID-4 -303.94 16.40 -305.42 5941.31 5941.28 5941.33 -302.21 5941.58 5941.43 1.71 18.29 3.38 -302.09 14.05 2.91 -306.20 17.53 3.92 14.82 2.11 EVID-5 -244.62 5940.32 5940.57 5940.51 23.83 0.65 -246.12 25.89 2.65 -242.99 21.48 5940.38 2.94 -246.02 24.29 5940.83 2.00 -242.91 22.64 1.97 VEH-POS -397.78 349.82 5963.07 1.06 -398.78 5963.29 1.75 -396.26 347.34 5962.63 2.10 -397.78 5962.55 1.46 -395.30 346.86 5963.25 2.87 1.28 AVG (in) 2.54 AVG (in) 2.57 3.46 AVG (in) AVG (in) AVG (in) AVG (cm) 4.93 -0.10 -1.84 0.78 -0.42 -0.79 -0.36

Site 2: Known evidence locations

		Site-02	
	Х	Y	Z
EVID-1	-412.11	472.04	5982.41
EVID-2	-297.45	385.49	5985.15
EVID-3	-263.50	325.19	5985.88
EVID-4	-417.60	317.75	5982.23
EVID-5	-392.37	261.79	5982.54
VEH-POS	-570.61	204.78	6012.91
VEH-ROT	2.31	0.53	-159.91

Site 2: Evidence placements (one camera match)

		1		Dif		2		Dif		3		D:4		4		Dif		5		Dif
	х	Υ	Z	ווט	Х	Υ	Z	х	Υ	Z	Dif	х	Υ	Z L	DII	Х	Υ	Z	"	
EVID-1	-415.34	475.81	5982.87	4.99	-414.89	476.16	5982.68	4.98	-413.68	473.80	5982.77	2.39	-413.08	473.768	5982.7	2.01	-415.81	476.70	5982.86	5.98
EVID-2	-302.83	390.56	5985.26	7.39	-301.86	389.31	5984.76	5.84	-298.70	386.59	5985.22	1.66	-297.08	384.023	5984.7	1.58	-303.06	391.46	5985.28	8.19
EVID-3	-264.43	323.83	5984.88	1.92	-264.22	324.09	5984.67	1.78	-261.17	321.38	5985.02	4.55	-259.38	317.65	5984.65	8.68	-265.16	325.91	5985.02	2.00
EVID-4	-417.65	317.94	5981.87	0.42	-417.87	318.13	5981.61	0.78	-415.69	312.58	5981.82	5.53	-416.33	314.42	5981.71	3.60	-418.02	318.79	5982.07	1.14
EVID-5	-390.73	257.66	5981.52	4.56	-391.10	257.67	5981.26	4.50	-387.94	251.15	5981.53	11.57	-389.16	252.775	5981.34	9.65	-390.99	256.70	5981.69	5.35
VEH-POS	-568.63	196.76	6011.94	8.31	-568.41	200.94	6012.06	4.50	-569.09	205.23	6012.66	1.60	-569.09	205.225	6012.66	1.60	-568.41	201.99	6012.42	3.58
			AVG (in)	4.60			AVG (in)	3.73			AVG (in)	4.55			AVG (in)	4.52			AVG (in)	4.37
1			AVG (cm)	11.68			AVG (cm)	9.48	]		AVG (cm)	11.56			AVG (cm)	11.48			AVG (cm)	11.11
VEH-ROT	2.70	0.28	-160.30		3.50	0.69	-159.25		1.10	0.57	-159.59		1.10	0.57	-159.59		2.49	0.40	-158.91	
	0.40	-0.24	-0.38	0.34	1.19	0.17	0.67	0.67	-1.21	0.04	0.32	0.52	-1.21	0.04	0.32	0.52	0.18	-0.13	1.00	0.44

Site 2: Evidence placements (three camera matches)

		1		Dif		2		Dif		3		Dif				Dif				Dif
	х	Υ	Z	DII	х	Υ	Z DII	х	Υ	Z	ווט	х	Υ	Z	ווט	х	Υ	Z	"	
EVID-1	-413.57	471.47	5981.80	1.68	-412.73	473.02	5982.17	1.19	-412.99	471.80	5981.84	1.07	-412.96	471.52	5982.64	1.03	-413.05	471.59	5981.92	1.15
EVID-2	-298.63	384.68	5984.65	1.52	-297.52	386.77	5984.72	1.34	-298.53	385.75	5984.61	1.23	-296.57	385.79	5984.68	1.04	-297.21	385.25	5984.77	0.51
EVID-3	-264.27	324.65	5985.27	1.12	-263.32	326.08	5985.29	1.09	-263.97	325.68	5985.48	0.79	-263.63	324.46	5985.52	0.82	-265.11	325.03	5984.72	1.99
EVID-4	-416.68	317.20	5981.77	1.16	-416.79	317.79	5981.83	0.91	-417.63	318.11	5981.88	0.51	-416.42	316.51	5982.34	1.71	-417.88	317.48	5981.75	0.62
EVID-5	-391.64	261.20	5982.06	1.06	-391.11	261.88	5982.18	1.32	-391.76	263.03	5982.06	1.46	-391.28	261.45	5981.45	1.58	-391.88	261.70	5981.79	0.90
VEH-POS	-569.55	203.00	6012.13	2.21	-569.52	203.30	6012.27	1.94	-569.64	204.21	6012.60	1.16	-570.03	203.59	6012.64	1.34	-568.82	202.89	6011.48	2.97
			AVG (in)	1.46			AVG (in)	1.30			AVG (in)	1.04			AVG (in)	1.25			AVG (in)	1.35
ll .			AVG (cm)	3.71			AVG (cm)	3.30	1		AVG (cm)	2.64	1		AVG (cm)	3.18			AVG (cm)	3.44
VEH-ROT	2.11	0.66	-159.68		2.86	0.69	-158.88		2.08	0.31	-159.92		1.10	0.57	-159.13		2.48	0.42	-159.31	
	-0.20	0.13	0.23	0.19	0.55	0.16	1.03	0.58	-0.23	-0.21	0.00	0.15	-1.21	0.04	0.78	0.68	0.18	-0.11	0.61	0.30

Site 3: Known evidence locations

		Site-03	
	Х	Y	Z
EVID-1	-663.55	-383.39	6003.42
EVID-2	-655.70	-326.77	6004.77
EVID-3	-805.58	-410.51	6005.02
EVID-4	-817.99	-353.82	6006.21
EVID-5	-728.31	-194.66	6007.28
VEH-POS	-477.55	-361.30	6031.25
VEH-ROT	1.80	1.27	-2.94

Site 3: Evidence placements (one camera match)

		1		Dif		2		Dif		3		Dif		4		Dif		5		Dif
	х	Υ	Z	ווט	х	Υ	Z DII	х	Υ	Z	ווט	х	Υ	Z	DII	Х	Υ	Z	l Dii	
EVID-1	-666.24	-384.07	6004.27	2.90	-653.05	-377.54	6004.15	12.05	-669.31	-386.62	6004.08	6.64	-671.47	-385.35	6003.68	8.16	-661.37	-381.67	6003.64	2.79
EVID-2	-659.95	-329.26	6005.45	4.97	-646.36	-321.71	6005.45	10.65	-662.53	-330.73	6005.20	7.90	-666.38	-330.51	6004.73	11.31	-653.60	-325.46	6004.96	2.49
EVID-3	-803.57	-410.15	6005.87	2.22	-793.47	-405.00	6005.58	13.32	-809.41	-413.91	6005.48	5.14	-810.74	-411.17	6005.17	5.20	-802.36	-408.96	6005.20	3.58
EVID-4	-815.48	-354.97	6007.05	2.88	-805.79	-349.22	6006.79	13.05	-820.64	-357.48	6006.80	4.55	-822.64	-355.39	6006.34	4.91	-813.20	-352.40	6006.21	5.00
EVID-5	-732.18	-201.73	6007.93	8.09	-720.07	-193.65	6007.81	8.33	-734.16	-201.12	6007.78	8.73	-737.75	-200.89	6007.61	11.32	-726.89	-196.79	6007.33	2.56
VEH-POS	-488.96	-369.74	6030.43	14.22	-471.00	-357.97	6030.88	7.36	-487.60	-368.77	6030.51	12.55	-491.74	-368.72	6030.45	16.03	-478.91	-362.26	6030.49	1.83
			AVG (in)	5.88			AVG (in)	10.79			AVG (in)	7.58			AVG (in)	9.49			AVG (in)	3.04
			AVG (cm)	14.93			AVG (cm)	27.42			AVG (cm)	19.26			AVG (cm)	24.10			AVG (cm)	7.73
VEH-ROT	1.88	1.51	-2.61		1.93	0.84	-1.72		1.75	1.00	-2.79		1.75	1.10	-2.29		2.30	0.80	-1.36	
	0.08	0.24	0.33	0.22	0.13	-0.43	1.22	0.59	-0.06	-0.27	0.15	0.16	-0.06	-0.17	0.65	0.29	0.50	-0.46	1.58	0.85

Site 3: Evidence placements (three camera matches)

2																					
Kes					Dif		2		Dif		3		Dif				Dif				Dif
TS		Х	Υ	Z	Dii	Х	Υ	Z	ווט	Х	Υ	Z	Dii	Х	Υ	Z	ווט	Х	Υ	Z	""
ignt	EVID-1	-664.58	-383.99	6003.91	1.29	-665.50	-385.20	6004.03	2.73	-669.14	-387.82	6004.05	7.16	-672.33	-387.19	6003.70	9.57	-666.22	-388.24	6004.33	5.61
₽ 1	EVID-2	-656.35	-327.46	6005.11	1.00	-657.98	-328.89	6005.26	3.15	-661.61	-330.93	6005.21	7.24	-664.09	-330.58	6004.82	9.21	-657.46	-330.15	6005.57	3.89
7	EVID-3	-804.00	-410.47	6005.35	1.62	-804.54	-411.37	6005.50	1.44	-808.56	-414.32	6005.47	4.86	-811.41	-413.01	6005.24	6.34	-809.14	-415.28	6005.45	5.96
onal.	EVID-4	-816.61	-355.11	6006.54	1.91	-817.12	-355.73	6006.76	2.17	-821.42	-359.39	6006.77	6.55	-823.98	-357.96	6006.33	7.28	-821.91	-358.22	6006.65	5.91
atic	EVID-5	-727.90	-197.61	6007.66	3.00	-729.81	-200.09	6007.75	5.66	-732.66	-201.78	6007.78	8.36	-736.46	-199.44	6007.83	9.46	-731.53	-199.22	6008.15	5.65
erne	VEH-POS	-479.46	-362.97	6030.99	2.55	-481.45	-364.32	6031.01	4.94	-485.14	-366.66	6031.01	9.29	-486.05	-366.06	6031.22	9.74	-480.01	-366.88	6031.79	6.12
uge l				AVG (in)	1.90			AVG (in)	3.35			AVG (in)	7.24			AVG (in)	8.60			AVG (in)	5.52
Ū.				AVG (cm)	4.82			AVG (cm)	8.50			AVG (cm)	18.40			AVG (cm)	21.85			AVG (cm)	14.03
N A																					
9	VEH-ROT	0.97	1.72	-3.11		2.01	1.40	-2.91		1.56	1.39	-2.57		1.75	0.71	-2.73		1.74	1.23	-3.20	
7		-0.84	0.45	-0.16	0.48	0.21	0.13	0.03	0.12	-0.25	0.12	0.37	0.25	-0.06	-0.56	0.21	0.28	-0.06	-0.04	-0.26	0.12

<sup>© 2019</sup> SAE International. All Rights Reserved.

<sup>© 2019</sup> SAE International. All rights reserved. No part of this publication may be reproduced, stored in a retrieval system, or transmitted, in any form or by any means, electronic, mechanical, photocopying, recording, or otherwise, without the prior written permission of SAE International.